CHAPTER 2

NUMERICAL RECONSTRUCTION OF SCALAR-VALUED LOCALIZED WAVE PULSES GENERATED FROM DYNAMIC APERTURE ANTENNAS

2.1 Introductory Remarks on Localized Wave Pulses

The possibility of exact solutions of the scalar wave equation that describe localized slowly decaying transmission of energy in space-time has been suggested by several groups in recent years [1-137]. These exact solutions [focus wave modes (FWM), modified power spectrum pulse (MPS), X waves, etc.], termed localized waves (LWs), can be obtained, among various methods, by means of two fundamental superposition schemes: the bidirectional and the boost variable representation [24,131].

The main characteristics properties of localized wave solutions can be summarized as follows:

(a) They are ultra-wideband, carrier-free pulses, compact in space and time;
(b) They are nonseparable functions of space and time;
(c) They consist of highly focused central portions embedded in sparse extended backgrounds;
(d) Ideal (nonrealizable) LWs propagate without any distortion, or with only local deformations;
(e) Finite energy LWs have large focusing depths and extended ranges of localization;
(f) Very close approximations to finite energy LWs can be launched causally from *dynamic aperture antennas*; the latter are characterized by time-varying effective radii;
(g) LWs display a strong coupling between their spatial and temporal spectral components. As they travel in the near-to-far region, the depletion of their spectral

content is different from that of quasi-monochromatic or broadband Gaussian pulses launched from static apertures.

Due to the aforementioned properties, LW pulses may have potential applications in different research areas, e.g., remote sensing, imaging, medical radiology, tissue characterization, impulse radar, nondestructive evaluation, plasma physics, directed energy transfer and secure communication. Experimental measurements confirming the feasibility of acoustic directed energy pulse trains (ADEPTs) for ultrasonic wave propagation in water were reported by Ziolkowski *et al*. [28,33]. In that experiment, localized waves were generated by an acoustical line array and were detected by a pseudopoint receiver. The measurements yielded both the amplitude and phase of the pressure field as a function of time. In a separate acoustic experiment [73], the backscattering properties of a MPS pulse incident on steel and aluminum spheres were used to extract target parameters (e.g., the radii and material properties of the spheres.) In that case, the MPS pulse was launched synthetically using a hydrophone system. Bandlimited X waves produced with an acoustic annular array transducer were used by Lu and Greenleaf [60] in experiments involving medical imaging. The time history for each annulus was first determined from the incident field; then a polynomial waveform synthesizer was used to generate the broadband signals required as inputs to the array elements. A demonstration of the LW effect in the optical frequency regime was reported recently by Sonajalg *et al*. [126].

2.2 Radiated Wavefield

Consider the three-dimensional scalar wave equation (SWE)

$$\left(\nabla^2 - \frac{1}{c^2}\frac{\partial^2}{\partial t^2}\right)\Psi(\mathbf{r},t) = 0 \; ; \; \mathbf{r} = (x,y,z), \tag{2.2.1}$$

where $\Psi(\mathbf{r},t)$ denotes the scalar-valued wavefield and c is the speed of propagation. Several types of exact localized wave solutions to the homogenous scalar wave equation (2.2.1) are known. Some of these LW solutions are not causal. This is the case for the FWM and MPS pulses, but not for the X wave. Our goal in this section is to examine various formulations that will allow us to compute purely causal or almost causal versions of such localized wave solutions in the region $z > 0$ given information about the wavefield distribution, as well as its time derivative and its normal derivative, at the aperture plane $z = 0$ as a function of x, y and t. Assuming an axisymmetric wavefield, viz., $\Psi(\mathbf{r},t) = \Psi(\rho,z,t)$, where $\rho = \sqrt{x^2 + y^2}$, solutions satisfying Eq. (2.2.1) can be obtained by means of four distinct representations:

(a) The positive Frequency Weyl representation [24,106]:

$$\Psi(\rho,z,t) = \frac{1}{2\pi}\int_0^\infty\int_0^\infty \phi_{ap}(\chi,\omega)\chi J_0(\chi\rho)e^{i\omega t}e^{-i\sqrt{(\omega/c)^2-\chi^2}z}d\chi d\omega\,. \tag{2.2.2}$$

Here, ω is the temporal angular frequency and χ is the transverse spatial spectral variable. Restricting $\sqrt{(\omega/c)^2-\chi^2}$ to real positive values ensures the forward illumination of the aperture at $z = 0$. As a consequence, the radiated field is causal and the integrand is expressed only in terms of outgoing Fourier components. Once the initial field distribution $\Psi(\rho,0,t) \Leftrightarrow \phi_{ap}(\chi,\omega)$ is defined on the aperture plane $z = 0$, the radiated field value in region $z > 0$ can be determined through this formulation.

(b) Huygens' construction [143]:

$$\Psi_H(\mathbf{r},t) = \frac{1}{4\pi}\iint_S dS'\left\{[\Psi]\frac{\partial}{\partial n'}\left(\frac{1}{R}\right) - \frac{1}{cR}\frac{\partial R}{\partial n'}\left[\frac{\partial \Psi}{\partial t}\right] - \frac{1}{R}\left[\frac{\partial \Psi}{\partial n'}\right]\right\}. \tag{2.2.3}$$

Here, Ψ is the scalar wavefield satisfying the SWE, n' is the inward unit vector normal to the surface S and R is the distance between the source point (x', y', z') on S and the observing point (x, y, z) contained within it. The square bracket in (2.2.3) indicates that the function inside it is to be evaluated at the retarded time $t - R/c$. Huygens' construction form is convenient for the practical realization of LW pulses and transient beams due to its dependence on the source parameters. The interpretation of Eq. (2.2.3) is as follows: The construction of the wavefield $\Psi(\mathbf{r}, t)$ can be performed inside a volume enclosed by the surface S knowing the time derivative of Ψ, the normal derivative of Ψ and the value of Ψ on this surface. For our specific application, S consists of two surfaces: S_1, the plane $z = 0$, and a hemispherical surface S_2 in the region $z > 0$. Application of the radiation condition as $R \to \infty$ shows that the integration over S_2 vanishes. Account must also be taken of the fact that the illuminated finite aperture A is only a part of S_1. These considerations lead to the Kirchhoff representation

$$\Psi_H(\rho, z, t) = \frac{1}{4\pi} \int_A dS' \left\{ [\Psi] \frac{\partial}{\partial n'} \left(\frac{1}{R} \right) - \frac{1}{cR} \frac{\partial R}{\partial n'} \left[\frac{\partial \Psi}{\partial t} \right] - \frac{1}{R} \left[\frac{\partial \Psi}{\partial n'} \right] \right\}. \tag{2.2.4}$$

In Appendix 2-A we show the equivalence of the Huygens representation and the positive frequency Weyl representation. This means that the radiated fields based on Huygens' construction are completely causal.

(c) The Rayleigh-Sommerfeld Integral II Representation [153,154]:

$$\Psi_{RSII}(\rho, z, t) = \frac{1}{2\pi} \int_A dS' \left\{ [\Psi] \frac{\partial}{\partial n'} \left(\frac{1}{R} \right) - \frac{1}{cR} \frac{\partial R}{\partial n'} \left[\frac{\partial \Psi}{\partial t} \right] \right\}. \tag{2.2.5}$$

In Appendix 2-B we show the equivalence between the Weyl representation and the Rayleigh Sommerfeld integral II representation, as long as the wavefield Ψ contains only causal components.

(d) The Rayleigh-Sommerfeld Integral I Representation [154]:

$$\Psi_{RSI}(\mathbf{r},t) = \frac{1}{2\pi}\int_A dS' \left\{ -\frac{1}{R}\left[\frac{\partial \Psi}{\partial n'}\right]\right\}. \tag{2.2.6}$$

The equivalence between the Weyl and Rayleigh-Sommerfeld integral I representations under the constraint that the wavefield Ψ contains only causal components is established in Appendix 2-C.

In summary, Huygens' representation filters out any acausal components of the wavefield Ψ. This is not true for the Rayleigh-Sommerfeld integral representations I and II. Therefore, certain precautions must be taken when they are used in conjunction with wavefields Ψ containing acausal components, e.g., the MPS pulse. It should be noted that Huygens' construction given in Eq. (2.2.4) is the average of the Rayleigh-Sommerfeld integral I, II representations.

2.3 Generation of Infinite Energy Localized Waves

Based on the positive frequency Weyl representation [cf. Eq. (2.2.2)], a real-valued, azimuthally symmetric excitation field on the aperture plane $z = 0$ has the form

$$\Psi_i(\rho,t) = \mathrm{Re}\left\{\hat{\Psi}_i(\rho,t)\right\}, \tag{2.3.1}$$

$$\hat{\Psi}_i(\rho,t)=\left[\frac{1}{2\pi}\int_0^{\infty}d\chi\int_0^{\infty}d\omega\hat{\phi}(\chi,\omega)\chi J_0(\chi\rho)e^{i\omega t}e^{-i\left(\sqrt{(\omega/c)^2-\chi^2}\right)z}\right]_{z=0}. \tag{2.3.2}$$

We introduce two distinct spectra as follows [43,96]:

$$\hat{\phi}_{FWM}(\chi,\omega)=\frac{1}{4}\delta\left[\omega-\left(\left(\chi^2/4\beta\right)+\beta\right)c\right]e^{-\chi^2 a_1/4\beta}, \tag{2.3.3}$$

$$\hat{\phi}_{XW}(\chi,\omega)=\frac{2\pi}{\chi}\delta\left[\omega-\chi y_0\right]e^{-\chi a_1};\ \ y_0=c\ \cosh\beta. \tag{2.3.4}$$

They correspond to the restriction on the $z=0$ plane of the two exact solutions of the homogeneous SWE, namely the Focus Wave Mode (FWM) and the X wave (XW). Inserting Eqs. (2.3.3) and (2.3.4) into Eq. (2.3.1), we obtain the following solutions:

$$\Psi_{FWM}(\mathbf{r},t)=\frac{\beta}{4\pi\left(a_1+i(z-ct)\right)}e^{-\beta\rho^2/\left(a_1+i(z-ct)\right)}e^{i\beta(z+ct)}+\varepsilon\left(\beta a_1\right), \tag{2.3.5}$$

$$\Psi_{XW}(\mathbf{r},t)=\frac{z_0}{\left[\left(z_0\rho\right)^2+\left(a_1z_0+i\left(z-ct\coth\beta\right)\right)^2\right]^{1/2}};\ z_0=1/\sinh\beta. \tag{2.3.6}$$

The first term on the right hand side of Eq. (2.3.5) is the source-free FWM pulse Ψ_{sf}; it consists of a complex envelope propagating in the positive $z-$direction with speed c, modulated by a plane wave propagating in the negative $z-$direction with speed c. The second term, of $O\left(\beta a_1\right)$ relative to the first one, arises because for the positive value of $\omega/c=\left(\chi^2/4\beta\right)+\beta$ the quantity $\sqrt{(\omega/c)^2-\chi^2}$ acquires either the value of $\left(\left(\chi^2/4\beta\right)-\beta\right)$ or

$-\left(\left(\chi^2/4\beta\right)-\beta\right)$, depending on whether $\chi > 2\beta$ or $\chi < 2\beta$, respectively. To ensure that Ψ_{FWM} resembles the source-free solution Ψ_{sf}, one must choose $\beta a_1 << 1$. With this restriction, the causal (forward) components of Ψ_{sf} dominate over the backward ones. The radius of the excitation wavefield at $z = 0$ is time dependent (dynamic aperture). It shrinks from an infinite radius at $t \to \infty$ to a minimum effective radius of order $\sqrt{a_1/\beta}$ at $t = 0$, then extends again to an infinite radius as $t \to \infty$. The energy content of the FWM is infinite because of the infinite time required for its excitation at the source plane. The envelope of the FWM propagates away from the aperture without any distortion. The entire pulse propagates in the $z \geq 0$ half-space undergoing only local deformations. Its initial amplitude at $z = 0$ is periodically recovered at distances $z = n\pi/\beta$, where n is integer.

The unidirectional solution given in Eq. (2.3.6) is identical to the zeroth order X wave derived by Lu and Greenleaf [59] if the following substitutions are made: $a_1 z_0 \to a_0/\cos\zeta$, $z_0\rho \to \rho\tan\zeta$, $c\coth\beta \to c/\cos\zeta$. In the notation used by Lu and Greenleaf, a_0 is a free parameter and ζ is the axicon angle. The energy content of the X wave is infinite because of the infinite time required for its excitation. In contrast to the FWM, the field amplitude of the X wave at the centroid $\left(\rho = 0, z = ct\coth\beta\right)$ holds constant for all distances z away from the aperture.

2.4 Generation of Finite Energy Localized Waves

In this section, we will discuss two distinct classes of finite energy localized waves. The first one is based on a superposition of elementary infinite energy localized waves. The second is obtained by limiting the illumination time of the aperture.

2.4.1 Superposition of Source-Free Focus Wave Mode

Ziolkowski [5,27] has shown that a finite energy solution to the homogeneous SWE can be obtained as a weighted superposition of FWMs. The modified power spectrum (MPS) pulse arises from such superposition; specifically,

$$\hat{\Psi}(\mathbf{r},t)=\frac{1}{(a_1+i\xi)}\int_0^{\infty} d\beta F(\beta)e^{-\beta s}\,, \tag{2.4.1.1}$$

where

$$s=\frac{\rho^2}{a_1+i\xi}-i\eta;\ \xi=z-ct\,,\ \eta=z+ct\,. \tag{2.4.1.2}$$

The substitution of the spectrum

$$F(\beta)=\left[p(p\beta-b)^{q-1}/\Gamma(q)\right]e^{a_2(p\beta-b)}H_s(\beta-b/p)\,, \tag{2.4.1.3}$$

where $H_s(\beta-b/p)$ denotes the Heaviside unit step function, yields the following explicit closed form expression for the MPS pulse:

$$\hat{\Psi}_{MPS}(\mathbf{r},\mathrm{t})=\frac{1}{(a_1+i\xi)\left((s/p)+a_2\right)^q}e^{-bs/p}\,. \tag{2.4.1.4}$$

Without loss of generality, we restrict our analysis to the case $q=1$, for which

$$\hat{\Psi}_{MPS}(\mathbf{r},\mathrm{t})=\frac{p}{\left(\mathrm{r}^2+\left(a_1+i\mathrm{x}\right)\left(pa_2-i\mathrm{h}\right)\right)}e^{-\left(b\mathrm{r}^2/p\left(a_1+i\mathrm{x}\right)\right)}e^{ib\mathrm{h}/p}\,. \tag{2.4.1.5}$$

It is known that the source-free MPS pulse contains acausal components. However, by tweaking the parameters incorporated in the solution, we can obtain a predominantly causal solution.

At $z = 0$, the wavefield given in Eq. (2.4.1.5) takes the following form:

$$\hat{\Psi}_i(\rho, z=0, t) = \frac{p}{\left(\rho^2 + (a_1 - ct)(pa_2 - ict)\right)} e^{-b\rho^2/p(a_1 - ict)} e^{ibct/p}. \qquad (2.4.1.6)$$

The Fourier spectrum of this expression can be derived from its bidirectional representation [24] and is given explicitly as [159]

$$\phi(\omega, \chi) = \frac{\pi p}{\sqrt{\left((\omega/c)^2 - \chi^2\right)}} \Lambda(\omega, \chi), \qquad \chi < \frac{\omega}{c} < \frac{p}{b}\left[\frac{\chi^2}{4} + \frac{b^2}{p^2}\right],$$
$$= 0, \qquad \text{otherwise,} \qquad (2.4.1.7a)$$

where

$$\Lambda(\omega, \chi) = e^{ba_2} e^{-\left(\omega/c + \sqrt{(\omega/c)^2 - \chi^2}\right)a_2/2} e^{-\left(\omega/c - \sqrt{(\omega/c)^2 - \chi^2}\right)pa_2/2}. \qquad (2.4.1.7b)$$

If the expression given in Eq. (2.4.1.6) is used to illuminate a flat aperture situated at $z = 0$, it can be established [159] that the field radiated into the $z > 0$ half-space is approximately equal to $\Psi_{MPS}(\mathbf{r}, t)$ as long as $pa_2 >> a_1$. This constraint is needed in order to minimize the acausal (backward propagating components) present in the solution given in Eq. (2.4.1.5). This is especially true around the highly focused central portion of the field. It follows from Eq. (2.4.1.5) that the amplitude of the MPS at observing points

$z > pa_2/2$ decays as $1/z$. The radius of the focused region of the MPS pulse is equal to $\sqrt{pa_1/b}$ and the initial amplitude at the pulse center is recovered periodically at distances $z = np/b$, n being any positive integer.

2.4.2 Time-Limited Excitation Wavefields

A finite energy, causal version of the FWM can be obtained using a Gaussian time window in order to turn off the illumination of the source plane after a certain time $|t| = 4T$. We choose, specifically, the time-limited FWM excitation field [106]

$$\hat{\Psi}_{TLFWM}(\rho,t) = \frac{\beta}{\pi(a_1 - ict)} e^{-\left(\beta\rho^2/(a_1 - ict)\right)} e^{i\beta ct} e^{-t^2/4T^2}. \qquad (2.4.2.1)$$

This is precisely the FWM at $z = 0$ multiplied by the Gaussian time window. The time-dependent radius of the excitation field and its maximum and minimum values can be deduced from the exponential factor [99,106]; they are given specifically as

$$R(t) = \frac{c|t|}{\sqrt{\beta a_1}}; \quad R_{\min} = \sqrt{\frac{a_1}{\beta}}; \; R_{\max} = \frac{4cT}{\sqrt{\beta a_1}}. \qquad (2.4.2.2)$$

The Fourier spectrum of the excitation field in Eq. (2.4.2.1) is given by

$$\phi(\chi,\omega) = \hat{\delta}(\omega - \omega_0(\chi); T) e^{-\chi^2 a_1/4\beta}; \; \omega_0(\chi) = (\chi^2/4\beta) + \beta, \qquad (2.4.2.3)$$

where

$$\hat{\delta}\left(\omega-\omega_0(\chi);T\right)=\frac{T}{\sqrt{\pi}}e^{-T^2\left(\omega-\omega_0(\chi)\right)^2}. \tag{2.4.2.4}$$

Along the same lines, the spectrum of the finite time X wave on the aperture plane $z = 0$ is chosen as

$$\hat{\phi}_{TLXW}(\chi,\omega)=\frac{2\pi}{\chi}\ e^{-\chi a_1}\hat{\delta}\left(\omega-\chi y_0\right);\ y_0 = c\cosh\beta, \tag{2.4.2.5}$$

where

$$\hat{\delta}\left(\omega-\chi y_0\right)=\frac{T}{\sqrt{\pi}}e^{-T^2\left(\omega-\chi y_0\right)^2}. \tag{2.4.2.6}$$

The corresponding space-time distribution at the aperture plane is given by

$$\hat{\Psi}_i(\rho,t)=\frac{e^{-t^2/4T^2}}{\left[\rho^2+\left(a_1-iy_0t\right)^2\right]^{1/2}}. \tag{2.4.2.7}$$

Finite energy solutions corresponding to the time-limited FWM and X wave excitations can be obtained by substituting Eqs. (2.4.2.3) and (2.4.2.5) into Eq. (2.2.2), viz.,

$$\Psi_{TLFWM}(\mathbf{r},t)=\frac{1}{2\pi}\int_0^\infty\int_0^\infty\frac{T}{\sqrt{\pi}}e^{-T^2\left(\omega-\omega_0(\chi)\right)^2}e^{-\chi^2/4\beta}\chi J_0(\chi\rho)e^{i\omega t}e^{-i\sqrt{(\omega/c)^2-\chi^2}z}d\chi d\omega, \tag{2.4.2.8}$$

$$\Psi_{TLXW}(\mathbf{r},t)=\frac{1}{2\pi}\int_0^\infty\int_0^\infty\frac{2\pi T}{\chi\sqrt{\pi}}e^{-T^2\left(\omega-\chi y_0\right)^2}e^{-\chi a_1}\chi J_0(\chi\rho)e^{i\omega t}e^{-i\sqrt{(\omega/c)^2-\chi^2}z}d\chi d\omega. \tag{2.4.2.9}$$

The Weyl representations of the TLFWM and the TLXW given in Eqs. (2.4.2.8) and (2.4.2.9), respectively, will be computed numerically in the sequel. In addition, these two representations will be used to obtain the corresponding wavefields, their time derivatives and their normal derivatives on the aperture plane $z = 0$. This information will be used in conjunction with the Huygens and Rayleigh-Sommerfeld integral I, II representations in order to obtain numerically the wavefields in the $z \geq 0$ half-space. This procedure will be repeated for the MPS pulse. Once the solutions are known in the region $z \geq 0$, all the propagation characteristics of the radiated wavefields, e.g., decay of the centroids, spatial spectra, diffraction lengths, etc. can be analyzed.

The positive frequency Weyl representation provides explicit expressions for the axial and transverse wavefield distributions. However, it does not lend itself to the physical realization of time-space aperture sources capable of generating LW pulse solutions propagating in the $z \geq 0$ half-space. The main purpose of using the reconstruction procedures embodied in the Huygens and Rayleigh-Sommerfeld integral I, II representations is to focus on the possibility of using space-time sources on the aperture plane to generate LW pulses in the region $z \geq 0$.

2.5 Numerical Implementation of the Huygens and Rayleigh-Sommerfeld Integral I, II Representations

Numerical implementation of Huygens' construction, as well as Rayleigh-Sommerfeld's integral I and II representations, for observation points along the $z-$axis $(\rho = 0)$ can be carried out using the following discrete forms:

$$\Psi_H(0,z,t) = \sum_{n=1}^{N} \frac{A_n}{4\pi R_n} \left\{ \left[\partial_{z'}\Psi\right] - \left[\partial_{ct'}\Psi\right] \frac{z - z_0}{R_n} - [\Psi] \frac{z - z_0}{R_n^2} \right\}, \tag{2.5.1}$$

$$\Psi_{RSI}(0,z,t) = \sum_{n=1}^{N} \frac{A_n}{2\pi R_n} \left\{ \partial_{z'} \Psi \right\}, \tag{2.5.2}$$

$$\Psi_{RSII}(0,z,t) = \sum_{n=1}^{N} \frac{A_n}{2\pi R_n} \left\{ \left[\partial_{ct'} \Psi \right] \frac{z - z_0}{R_n} + [\Psi] \frac{z - z_0}{R_n^2} \right\}. \tag{2.5.3}$$

In these expressions, A_n is the area of the annular section labeled n, N is the number of the annular sections, $\rho'_n = n\Delta\rho'$ is the radius of the annular section labeled n, $\Delta\rho'$ is the width of an annular section and z is the distance at which the field of the radiated pulse is reconstructed. The distance from the source point to the observation point $(\rho = 0)$ can be evaluated by

$$R_n = \sqrt{\left(n\Delta\rho'\right)^2 + \left(z - z_0\right)^2}\,. \tag{2.5.4a}$$

A geometrical configuration of the source plane and the discrete annular sections is shown in Fig. 4.1.

The time history is calculated at certain instances expressed as the following retarded times:

$$t'_{n,j} = t_j + \frac{z - z_0}{c} - \frac{R_n}{c}. \tag{2.5.4b}$$

Here, t_j is the time incrementation around z/c. To use the reconstruction formulas, we first calculate the fields and their derivatives at the source plane, and then substitute their values at the retarded times $t'_{n,j}$.

It is important to illustrate the effect of the radiator elements, situated at different radial positions, on the field value at a specific range away from the aperture. This can be done by calculating the amplitude of the centroid of the pulse generated by a specific number of annular rings $m < N$. The parameter m specifies the position of the annular rings contributing to the field at the specific range.

2.6 Numerical Results

We consider, first, the infinite time FWM and the MPS pulse. As mentioned earlier, these two LWs are exact solutions to the homogeneous SWE, and both contain acausal components. The former has infinite and the latter finite energy content. We shall use the Huygens construction method to obtain causal versions of these two LWs. For comparison purposes, the initial excitations have the same temporal bandwidths, they attain equal focused waists and are applied to apertures having equal radii. For the MPS pulse we use the following parameter values: $a_1 = 2\times10^{-6}$ m, $a_2 = 0.1$ m, $b = 8000\ \mathrm{m}^{-1}$ and $p = 4000$. These values result in an excitation wavefield having a focused radius $R_{\min} = \sqrt{pa_1/b} = 10^{-3}\mathrm{m}$ and a maximum temporal frequency equal to $\left(\omega_{\max}/c\right) = 4/a_1 = 2\times10^{6}\,\mathrm{m}^{-1}$. The natural maximum cutoff radius has the value $R_{\max} = 2a_2\sqrt{pba_1} = 1.6$ m. For the FWM pulse we choose the parameters $a_1 = 2\times10^{-6}$ m and $\beta = 2\,\mathrm{m}^{-1}$. These values yield the same temporal bandwidth $\left(\omega_{\max}/c\right) = 4/a_1 = 2\times10^{6}\ \mathrm{m}^{-1}$ and minimum radius $R_{\min} = \sqrt{a_1/\beta} = 10^{-3}\mathrm{m}$. The decay rates of the amplitudes of the centroids of the two pulses are compared in Figs. (2.2a) and (2.2b), respectively, where the absolute values of the amplitudes are plotted as functions of z. The plots shown in the figures correspond to the fields generated by discrete concentric annular arrays having radii $R = 1$, 1.6, 2, 2.2 and 2.5 m. The width of each annular section is set equal to $\Delta\rho = 1\mathrm{mm}$. The decay of the

centroid of the FWM pulse, shown in Fig. 2.2a, displays a uniform increase in its focused range as the effective aperture radius R is increased. On the other hand, it is clear from Fig. 2.2b that the improvement in the performance of the MPS pulse is less pronounced once the radius of the aperture becomes larger than the natural cutoff radius $R_{\max} = 1.6$ m. This means that if we use an MPS aperture having $R > R_{\max}$, we are not utilizing the full size of the aperture efficiently.

Fig. 2.3 shows a comparison of the decay pattern of the TLFWM field computed directly from the positive frequency Weyl representation [cf. Eq. (2.4.2.8)], with parameters $cT = 10^{-3}$ m, $R_{\max} = 4cT/\sqrt{\beta a_1} = 2$ m, and that of a FWM pulse generated by means of Huygens' construction. We have chosen the radius of the array R to be equal to the natural cutoff radius of the TLFWM dynamic aperture $R_{\max} = 2$ m. It is clear, from the figure, that the TLFWM exhibits a faster decay in the near field. This may be attributed to the Gaussian turn off of the amplitude of the excitation wavefield. In such a case, the power of the illumination of the source is continuously reduced before the excitation field expands to illuminate the natural extension of the aperture $R_{\max}$. One should, also, note the faster decay of the FWM pulse generated from a circular array at farther distances. This may be explained as follows: Having a physical boundary is equivalent to illuminating a dynamic aperture by a wavefield whose ω-windows become wider for higher χ components [109,110]. This causes the decay rate to increase as the pulse travels to farther distances.

Next, we compare the decay rate of the exact MPS pulse to a fully causal MPS field obtained by the restriction $\chi > 2b/p$ in the spectrum [cf. Eq. (2.4.1.7)] and using only the positive root of $\sqrt{(\omega/c)^2 - \chi^2}$ in the positive frequency Weyl superposition given in Eq. (2.2.2). It is shown in Fig. 2.4 that for small ranges from the aperture the causal MPS

decay rate is identical to that of the exact MPS pulse. At farther distances, however, the causal MPS decay actually slows down. This indicates that the parameter tweaking $pa_2 >> a_1$ results in a predominantly forward traveling wavefield. The acausal components obviously do not support the forward traveling ones to the extent of slowing down their decay rate. Moreover, we know that the exact MPS pulse decays in the far-field region as $(1/z)$. Consequently, the rate of decay of the centroid of the causal MPS pulse, shown in Fig. 2.4, is slower than $(1/z)$ as the pulse propagates deeper in the far-field region.

The decay of the normalized field value of a zeroth-order X wave, computed by Huygens' construction method, is demonstrated in Fig. 2.5. It is seen that the decay becomes slower as the excitation time corresponding to the radius of the discrete arrays increases. The parameters used for the X wave are the following: $a_1 = 0.004\ \mathrm{m}^{-1}$, $\beta = 7.4$ and $c = 1500\ \mathrm{m/s}$. The variation of the field value with the distance z and the radius of the discrete arrays is shown in Fig. 2.6. As the effective radius of the aperture becomes larger, the decay rate slows down to zero. In other words, we obtain the physically unrealizable exact zeroth-order X wave solution.

As mentioned earlier, the source-free MPS pulse contains acausal components. However, by tweaking the parameters incorporated in the solution we obtain a predominantly causal solution. Huygens' construction filters out the incoming acausal components, and the generated field is totally causal. This is not the case for the Rayleigh-Sommerfeld integral I and II constructions. Nevertheless, the latter constructions are useful in checking the effectiveness of the "parameter tweaking" criterion. In particular, if such an argument is true, one should not be able to detect any differences in the fields generated using the Rayleigh-Sommerfeld integral I and II representations when compared to those generated by Huygens' construction. As an illustration, we choose a MPS pulse with parameters such that predominance of the outgoing (causal) field components is ensured; specifically,

we set $a_2 = 1\,\text{cm}$, $a_1 = 1.667\times10^{-3}\,\text{cm}$, $p = 6\times10^{15}$ and $b = 1\times10^{10}\ \text{cm}^{-1}$. The reconstructed pulses at $1\,\text{km}$ and $10\,\text{km}$ are shown in Figs. (2.7a) and (2.7b), respectively. These figures show the time history of the exact MPS pulse and one reconstructed using the Rayleigh-Sommerfeld integral I representation. The finite radii of their sources are equal to 0.5 and 5 m, respectively. The pulses reconstructed using the other two methods are indistinguishable from the ones in the figures. This indistinguishabilty of the fields resulting from the three methods confirms the validity of the "parameter tweaking" approach when one tries to construct causal LW solutions. The same conclusion was reached earlier by Ziolkowski who compared the exact MPS pulse to one generated by Huygens' construction [27]. In Fig. 2.8 we display the decay of the centroid of the MPS pulse as a function of the distance z. The effective contribution of the circular array elements to the field amplitude at different distances is given in Fig. 2.9.

As a final example, we consider the case of the second derivative X-wave pulse, which can be written as

$$\Psi_{2XW}(\rho,z,t) = \frac{2\left(a_0 - i\left(z\cos\zeta - ct\right)\right)^2 - \left(\rho\sin\zeta\right)^2}{\left(\left(a_0 - i\left(z\cos\zeta - ct\right)\right)^2 + \left(\rho\sin\zeta\right)^2\right)^{5/2}}. \tag{2.6.1}$$

Unlike the MPS pulse, the components of this wavefield are all causal. In this case, we compare the time history of the reconstructed pulse to the source-free solution. The pulses are reconstructed at $z = 200$ mm from a finite source of radius $R = 30$ mm using the parameter values $a_0 = 0.35\,\text{mm}$, $\zeta = 0.115$ rad and $c = 1500$ m/s. The fields reconstructed using the three techniques are identical. The one plotted in Fig. 2.10 is calculated using the Rayleigh-Sommerfeld integral I representation. One should expect such a resemblance because the three construction methods yield identical radiated fields when the Fourier components of the excitation wavefield are all diverging from the aperture (causal).

Furthermore, our analysis has also confirmed the capability of generating LW pulses with close resemblance to the exact ones by using discrete circular elements. In Fig. 2.11 we display the decay of the center of the second derivative X wave pulse as a function of the distance z.

2.7 Reconstruction of LW Pulses in the Frequency Domain

It is often convenient to carry out the reconstruction of LW pulses in the frequency domain, especially if the spectrum on the aperture plane is available as a function of ρ and $k = \omega/c$. The frequency domain formulations of Huygens' construction and the Rayleigh-Sommerfeld integral I and II representations assume the forms

$$\hat{\Psi}_{Huy}(\rho,z,k) = \frac{1}{2i\lambda}\int_0^{2\pi} d\phi' \int_0^{D/2} \rho' d\rho' \hat{\Psi}(\rho',\phi',k)\frac{e^{-ikR}}{R^2}z + \frac{1}{4\pi}\int_0^{2\pi} d\phi' \int_0^{D/2} \rho' d\rho' \hat{\Psi}(\rho',\phi',k)\frac{e^{-ikR}}{R^3}z + \frac{1}{4\pi}\int_0^{2\pi} d\phi' \int_0^{D/2} \rho' d\rho' \left.\frac{\partial\hat{\Psi}(\rho',\phi',z',k)}{\partial z'}\right|_{z'=0} \frac{e^{-ikR}}{R}; \quad (2.7.1)$$

$$\hat{\Psi}_{RSII}(\rho,z,k) = \frac{1}{i\lambda}\int_0^{2\pi} d\phi' \int_0^{D/2} \rho' d\rho' \hat{\Psi}(\rho',\phi',k)\frac{e^{-ikR}}{R^2}z + \frac{1}{2\pi}\int_0^{2\pi} d\phi' \int_0^{D/2} \rho' d\rho' \hat{\Psi}(\rho',\phi',k)\frac{e^{-ikR}}{R^3}z; \quad (2.7.2)$$

$$\hat{\Psi}_{RSI}(\rho,z,k) = \frac{1}{2\pi}\int_0^{2\pi} d\phi' \int_0^{D/2} \rho' d\rho' \left.\frac{\partial\hat{\Psi}(\rho',\phi',z',k)}{\partial z'}\right|_{z'=0} \frac{e^{-ikR}}{R}, \quad (2.7.3)$$

where λ is the wavelength $(k = 2\pi/\lambda)$, D is the diameter of the circular radiator on the aperture plane $z = 0$ and R is the distance between the point at which the reconstructed pulse is required (observing point) and a source point. These forms can be computed numerically for each frequency value and at a specific observing point in order to obtain

the spectrum of the radiated pulse. In the presence of axisymmetry (no dependence on ϕ'), the double integration in Eqs. (2.7.1)-(2.7.3) reduces to a single integration over ρ'. For illustrative purposes, consider the temporal spectrum corresponding to the second derivative X wave, viz.,

$$\hat{\Psi}_{2nd}(\rho,\phi,z,k) = \frac{2\pi}{c}\left(\frac{\omega}{c}\right)^2 J_0(k\rho\,\sin\zeta)H(k)e^{-k\left(a_0 - iz\cos\zeta\right)}\,, \tag{2.7.4}$$

where a_0 is an arbitrary constant, ζ is the axicon angle and $H(k)$ denotes the Heaviside unit step function. This spectrum contains contributions from both low and high frequency components. The energy content of the space-time second derivative X wave is infinite. To generate a finite energy version of this pulse, we multiply the spectrum given in Eq. (2.7.4) by a band-limited function $B(k)$, corresponding to the transfer function of a realistic transducer. We have, then,

$$\hat{\Psi}(\rho,\phi,z,k) = B(k)\hat{\Psi}_{2\,XW}(\rho,\phi,z,k)\,. \tag{2.7.5}$$

The space-time pulse is obtained as

$$\Psi(\rho,z,t) = F^{-1}\left[B(\omega/c)\hat{\Psi}_{2nd}(\rho,z,k)\right] = F^{-1}[B(k)] \otimes F^{-1}\left[\hat{\Psi}_{2nd}(\rho,z,\omega/c)\right]. \tag{2.7.6}$$

where F^{-1} denotes the inverse fast Fourier transform and $\otimes$ convolution in time.

The spectrum $\hat{\Psi}(0,z,\omega/c)$ and the time history $\Psi(0,z,t)$ along the $z-$axis $(\rho = 0)$ and at a distance $z = 20$ cm have been calculated using Eqs. (2.7.4)-(2.7.6) for the second derivative X-wave with parameter values $\zeta = 6.6^o$, $a_0 = 0.35$mm, $c = 1500$ m/s and a flat window function $B(\omega/c) = a_0$. These results are compared in Fig. 2.12 with those obtained using the frequency domain Rayleigh-Sommerfeld integral II representation given

in Eq. (2.7.2), with $D/2 = 3$ cm and $\Delta f \equiv \Delta\omega/2\pi$ =50 KHz. It is clear that the exact results match very well the reconstructed ones, primarily because the second derivative X wave contains no acausal components.

2.8 Concluding Remarks

In this chapter, we have carried out a detailed comparison of three well-known field construction methods, both in the time and frequency domain. We claim that a notable difference among them depends on how they deal with acausal incoming field components incorporated in their excitation wavefields. This can occur if one uses source excitations that are superpositions of source-free FWM solutions [27]. An example of this category is the MPS pulse. We have shown in Appendix 2-A that even if the excitation wavefield contains acausal components, the radiated field is totally causal if one uses Huygens' construction. This is the case because such an approach filters out the acausal components. On the other hand, the Rayleigh-Sommerfeld integral I and II constructions support the acausal components in the radiated field [cf. Appendices 2-B and 2-C]. It has been previously argued that tweaking the parameters of the MPS pulse can make the outgoing (causal) components predominant in the radiated field [106]. As such, the radiated field should resemble the corresponding source-free pulse. This has been confirmed by this work. Furthermore, we have shown that the acausal components can be made so small that the fields reconstructed using the Rayleigh-Sommerfeld integral I and II representations are indistinguishable from those reconstructed from Huygens' formula. If the acausal components are negligible, or we are sure that the excitation field is completely causal, then choosing among the three formulas is a matter of preference. Huygens' construction is the most complicated; the choice between the other two formulas depends on which derivatives are easier to evaluate.

Appendix 2-A

The Equivalence of the Huygens and Weyl Representations of the Solution to the 3-D Scalar Wave Equation

Consider the scalar wave equation

$$\nabla^2\Psi - \frac{1}{c^2}\frac{\partial^2\Psi}{\partial t^2} = 0. \tag{2-A.1}$$

The Huygens representation of the field $\Psi(\mathbf{r},t)$ inside a wave front surface (zero field outside) is given as [143]

$$\Psi(\mathbf{r},t) = \frac{1}{4\pi}\oint_S dS'\left\{\Psi(\mathbf{r}',t')\frac{\partial}{\partial n'}\left(\frac{1}{R}\right) - \frac{1}{cR}\frac{\partial R}{\partial n'}\frac{\partial\Psi(\mathbf{r}',t')}{\partial t'} - \frac{1}{R}\frac{\partial\Psi(\mathbf{r}',t')}{\partial n'}\right\}_{t'=t-R/c}, \tag{2-A.2}$$

where $R = |r - r'|$. Choosing S to be the aperture plane $z = 0$ and assuming axisymmetry $\left[\Psi(\mathbf{r},t) = \Psi(\rho,z,t)\right]$, the Huygens representation specializes to

$$\Psi(\rho,z,t) = \frac{1}{4\pi R}\int_0^{2\pi} d\phi'\int_0^{\infty}\rho' d\rho'\left\{\left.\frac{-\partial\Psi(\rho',z',t')}{\partial z'}\right|_{z'=0} + \Psi(\rho',0,t')\frac{z}{R^2} + \frac{z}{cR}\frac{\partial\Psi(\rho',0,t')}{\partial t'}\right\}_{t'=t-R/c} \tag{2-A.3}$$

where $R = \sqrt{\rho^2 + \rho'^2 - 2\rho\rho'\cos\phi' + z^2}$. Our goal is to show that (2-A.3) is equivalent to the positive frequency Weyl representation

$$\Psi(\rho,z,t) = \frac{1}{2\pi}\int_0^{\infty}\int_0^{\infty}\phi_{ap}(\chi,\omega)\chi J_0(\chi\rho)e^{i\omega t}e^{-i\sqrt{(\omega/c)^2-\chi^2}\,z}d\chi d\omega,\ z > 0, \tag{2-A.4}$$

where $\phi_{ap}(\chi,\omega)$ denotes the spatio-temporal spectrum on the aperture plane $(z = 0)$, viz., $\phi_{ap}(\chi,\omega) \Leftrightarrow \Psi(\rho,0,t)$. We use, next, (2-A.4) in order to compute the value of the scalar

field and its space and time derivatives required in the Huygens representation given in (2-A.3). Specifically, we obtain

$$\Psi(\rho',0,t') = \frac{1}{2\pi}\int_0^\infty d\omega \int_0^\infty d\chi\, \chi J_0(\chi\rho') e^{i\omega t'} \phi_{ap}(\chi,\omega), \tag{2-A.5}$$

$$\frac{\partial\left(\Psi(\rho',0,t')\right)}{\partial t'} = \frac{1}{2\pi}\int_0^\infty d\omega \int_0^\infty i\omega\chi d\chi J_0(\chi\rho') e^{i\omega t'} \phi_{ap}(\chi,\omega), \tag{2-A.6}$$

$$\left.\frac{\partial\left(\Psi(\rho',z',t')\right)}{\partial z'}\right|_{z'=0} = \frac{1}{2\pi}\int_0^\infty d\omega \int_0^\infty \left(-i\sqrt{(\omega/c)^2-\chi^2}\right)\chi d\chi J_0(\chi\rho') e^{i\omega t'} \phi_{ap}(\chi,\omega). \tag{2-A.7}$$

Substituting these expressions into (2-A.3), we have

$$\Psi(\rho,z,t) = \frac{1}{4\pi}\int_0^{2\pi} d\phi' \int_0^\infty \rho' d\rho' \Psi_1(\rho',z,t'), \tag{2-A.8}$$

where

$$\Psi_1(\rho',z,t') = \frac{1}{2\pi}\int_0^\infty \chi d\chi J_0(\chi\rho') \int_0^\infty \phi_{ap}(\chi,\omega) e^{i\omega t'} \frac{1}{R}\left[i\sqrt{(\omega/c)^2-\chi^2} + \frac{i\omega z}{cR} + \frac{z}{R^2}\right]_{t'=t-R/c} d\omega \tag{2-A.9}$$

We use, next, the identity

$$\frac{\partial}{\partial z}\left[\frac{e^{-i\omega R/c}}{R}\right] = -\left[\frac{i\omega z}{cR^2} + \frac{z}{R^3}\right]e^{-i\omega R/c}. \tag{2-A.10}$$

Inserting (2-A.10) in (2-A.9), we obtain

$$\Psi_1(\rho',z,t-R/c) = \frac{1}{2\pi}\int_0^\infty \chi d\chi J_0(\chi\rho') \int_0^\infty \phi_{ap}(\chi,\omega)\left[\frac{i\sqrt{(\omega/c)^2-\chi^2}}{R} e^{i\omega R/c} - \frac{\partial}{\partial z}\left(\frac{e^{-i\omega R/c}}{R}\right)\right] d\omega. \tag{2-A.11}$$

Consider the identity given in Ref. [157], p. 435, viz.,

$$\frac{e^{-i\omega R/c}}{R} = \int_0^\infty \lambda d\lambda J_0\left(\lambda\rho^*\right) I(\lambda, z), \tag{2-A.12}$$

where $\rho^* = \sqrt{\rho^2 + \rho'^2 - 2\rho\rho'\cos\phi'}$ and

$$I(\lambda, z) = \frac{1}{\pi}\int_{-\infty}^{\infty} \frac{e^{-ik_z z}}{k_z^2 - \left[\left(\omega/c\right)^2 - \lambda^2\right]} dk_z . \tag{2-A.13}$$

The integration over k_z can be evaluated using Caushy's theorem with the residues [158] $k_z \to -\sqrt{\left(\omega/c\right)^2 - \lambda^2}$ for $z < 0$ and $k_z \to \sqrt{\left(\omega/c\right)^2 - \lambda^2}$ for $z > 0$. This leads to

$$I(\lambda, z) = -i\left[\frac{e^{-i|z|\sqrt{\left(\omega/c\right)^2 - \lambda^2}}}{\sqrt{\left(\omega/c\right)^2 - \lambda^2}}\right]. \tag{2-A.14}$$

Since we are interested in the region $z > 0$, we obtain

$$\frac{\partial I(\lambda, z)}{\partial z} = -e^{-iz\sqrt{\left(\omega/c\right)^2 - \lambda^2}} \tag{2-A.15}$$

and

$$i\sqrt{\left(\omega/c\right)^2 - \lambda^2}\, I(\lambda, z) = e^{-iz\sqrt{\left(\omega/c\right)^2 - \lambda^2}} . \tag{2-A.16}$$

We use, next, the identity

$$\frac{i\sqrt{\left(\omega/c\right)^2 - \chi^2}}{R} e^{-i\omega R/c} - \frac{\partial}{\partial z}\left(\frac{e^{-i\omega R/c}}{R}\right) = \int_0^\infty \lambda d\lambda J_0\left(\lambda\rho^*\right)\left[i\sqrt{\left(\omega/c\right)^2 - \chi^2}\, I(\lambda, z) - \left[-e^{-iz\sqrt{\left(\omega/c\right)^2 - \lambda^2}}\right]\right]. \tag{2-A.17}$$

Using (2-A.17) in conjunction with Eq. (2-A.11), we obtain

$$\Psi_1(\rho',z,t-R/c)=\frac{1}{2\pi}\int_0^\infty \chi d\chi J_0(\chi\rho)\int_0^\infty \phi_{ap}(\chi,\omega)e^{i\omega t}d\omega$$
$$\times\int_0^\infty \lambda d\lambda J_0(\lambda\rho^*)\left[i\sqrt{(\omega/c)^2-\chi^2}\,I(\lambda,z)+\left[e^{-iz\sqrt{(\omega/c)^2-\lambda^2}}\right]\right]. \tag{2-A.18}$$

When this expression is substituted into (2-A.8), the integration over ϕ' can be carried out by using Eq. (6.684.1) of Ref. [144],viz.,

$$\int_0^{2\pi} d\phi' J_0(\chi\rho^*)=\int_0^{2\pi} d\phi' J_0\left(\chi\sqrt{\rho^2+\rho'^2-2\rho\rho'\cos\phi'}\right)=2\pi J_0(\chi\rho')J_0(\chi\rho). \tag{2-A.19}$$

As a consequence,

$$\Psi(\rho,z,t)=\frac{1}{4\pi}\int_0^\infty \rho' d\rho'\frac{1}{2\pi}\int_0^\infty \chi d\chi J_0(\chi\rho')\int_0^\infty \phi_{ap}(\chi,\omega)e^{i\omega t}d\omega\int_0^\infty \lambda d\lambda 2\pi J_0(\lambda\rho)\times$$
$$J_0(\lambda\rho')\left[i\sqrt{(\omega/c)^2-\chi^2}\,I(\lambda,z)+\left[e^{-iz\sqrt{(\omega/c)^2-\lambda^2}}\right]\right]. \tag{2-A.20}$$

We use next the orthogonality property

$$\frac{\delta(\chi-\lambda)}{\lambda}=\int_0^\infty \rho' d\rho' J_0(\chi\rho')J_0(\lambda\rho'). \tag{2-A.21}$$

Substituting (2-A.21) in (2-A.20) and integrating over λ, we obtain

$$\Psi(\rho,z,t)=\frac{1}{4\pi}\int_0^\infty\int_0^\infty \chi d\chi J_0(\chi\rho)\phi_{ap}(\chi,\omega)e^{i\omega t}d\omega\times$$
$$\left[i\sqrt{(\omega/c)^2-\chi^2}\,I(\chi,z)+\left[e^{-iz\sqrt{(\omega/c)^2-\chi^2}}\right]\right] \tag{2-A.22}$$

From (2-A.16), we have

$$\left[i\sqrt{(\omega/c)^2-\chi^2}\right]I(\chi,z)=\left[e^{-iz\sqrt{(\omega/c)^2-\chi^2}}\right]. \tag{2-A.23}$$

Substituting (2-A.23) into (2-A.22), we obtain

$$\Psi(\rho,z,t)=\frac{1}{2\pi}\int_0^\infty\int_0^\infty \phi_{ap}(\chi,\omega)\chi J_0(\chi\rho)e^{i\omega t}e^{-i\sqrt{(\omega/c)^2-\chi^2}z}d\chi d\omega, \qquad \text{(2-A.24)}$$

which is the desired Weyl representation of the radiated field $(\omega/c>\chi)$ in the region $z>0$. This proof shows that Huygens' construction passes only the forward (causal) components even if the exciting field includes acausal ones.

Appendix 2-B

The Equivalence of the Rayleigh-Sommerfeld Integral I and Weyl Representations of the Solution of the 3-D Scalar Wave Equation

The Rayleigh-Sommerfeld integral I representation of the solution $\Psi(\mathbf{r},t)$ to the scalar wave equation [cf. Eq. (2-A.1)] inside a wavefront surface (zero field outside) is given as follows [153]:

$$\Psi(\mathbf{r},t) = \frac{1}{2\pi}\oint_S dS' \left\{ \frac{1}{R}\frac{\partial \Psi(\mathbf{r}',t')}{\partial n'} \right\}_{t'=t-R/c} . \tag{2-B.1}$$

Choosing S to be the aperture plane $z = 0$ and assuming axisymmetry $\left[\Psi(\mathbf{r},t) = \Psi(\rho,z,t)\right]$, (2-B.1) specializes to

$$\Psi(\rho,z,t) = \frac{1}{2\pi}\int_0^{2\pi} d\phi' \int_0^{\infty} \rho' d\rho' \frac{1}{R}\left\{ \left.\frac{\partial \Psi(\rho',z',t')}{\partial z'}\right|_{z'=0} \right\}_{t'=t-R/c} , \tag{2-B.2}$$

where $R = \sqrt{\rho^2 + \rho'^2 - 2\rho\rho'\cos\phi' + z^2}$. Our goal is to show that (2-B.2) is equivalent to the Weyl representation [cf.(2-A.4)], viz.,

$$\Psi(\rho,z,t) = \frac{1}{2\pi}\int_0^{\infty}\int_0^{\infty} \phi_{ap}(\chi,\omega)\chi J_0(\chi\rho) e^{i\omega t} e^{-i\sqrt{(\omega/c)^2-\chi^2}\,z} d\chi d\omega \, , z > 0 , \tag{2-B.3}$$

where $\phi_{ap}(\chi,\omega)$ denotes the spatio-temporal spectrum on the aperture plane $(z = 0)$ $\phi_{ap}(\chi,\omega) \Leftrightarrow \Psi(\rho,0,t)$. We use, next, (2-B.3) in order to compute the value of the quantity $(\partial/\partial z')\Psi(\rho',z,t')\big|_{z'=0}$ required in Rayleigh-Sommerfeld integral I representation. Specifically, we obtain

$$\left.\frac{\partial\left(\Psi\left(\rho',z',t'\right)\right)}{\partial z'}\right|_{z'=0}=\frac{1}{2\pi}\int_0^{\infty}d\omega\int_0^{\infty}\left(-i\sqrt{\left(\omega/c\right)^2-\chi^2}\right)\chi d\chi J_0\left(\chi\rho'\right)e^{i\omega t'}\phi_{ap}\left(\chi,\omega\right). \tag{2-B.4}$$

Substituting this expression into (2-B.2), we obtain

$$\Psi\left(\rho,z,t\right)=\frac{1}{4\pi}\int_0^{2\pi}d\phi'\int_0^{\infty}\rho' d\rho'\Psi_1\left(\rho',z,t'\right), \tag{2-B.5}$$

$$\begin{aligned}\Psi_1\left(\rho',z,t'\right)&=\frac{1}{2\pi}\int_0^{\infty}\chi d\chi J_0\left(\chi\rho'\right)\int_0^{\infty}\phi_{ap}\left(\chi,\omega\right)\frac{1}{R}\left[i\sqrt{\left(\omega/c\right)^2-\chi^2}e^{i\omega t'}\right]_{t'=t-R/c}d\omega\\&=\frac{1}{2\pi}\int_0^{\infty}\chi d\chi J_0\left(\chi\rho'\right)\int_0^{\infty}\phi_{ap}\left(\chi,\omega\right)e^{i\omega t}\frac{1}{R}\left[i\sqrt{\left(\omega/c\right)^2-\chi^2}\right]e^{-i\omega R/c}d\omega.\end{aligned} \tag{2-B.6}$$

Consider, next, the identity

$$\frac{e^{-i\omega R/c}}{R}=\int_0^{\infty}\lambda d\lambda J_0\left(\lambda\rho^*\right)I(\lambda,z), \tag{2-B.7}$$

where $\rho^*=\sqrt{\rho^2+\rho'^2-2\rho\rho'\cos\phi'}$ and

$$I(\mathrm{l},z)=\frac{1}{\mathrm{p}}\int_{-\infty}^{\infty}\frac{e^{-ik_z z}}{k_z^2-\left[\left(\mathrm{w}/c\right)^2-\mathrm{l}^2\right]}dk_z \tag{2-B.8}$$

According to the identity in Ref. [157], p.435, this integration yields

$$I\left(\lambda,z\right)=-i\left[\frac{e^{-i|z|\sqrt{\left(\omega/c\right)^2-\lambda^2}}}{\sqrt{\left(\omega/c\right)^2-\lambda^2}}\right]. \tag{2-B.9}$$

Substituting (2-B.9), for $z>0$, into (2-B.7) and the latter into (2-B.6), we obtain

$$\Psi_1(r',z,t-R/c)=\frac{1}{2p}\int_0^{\infty} c\,dc\,J_0(cr)\int_0^{\infty} f_{ap}(c,w)e^{iwt}dw$$
$$\times\int_0^{\infty} l\,dl\,J_0(lr^*)\left[i\sqrt{(w/c)^2-c^2}(-2pi)\frac{e^{-iz\sqrt{(w/c)^2-l^2}}}{2p\sqrt{(w/c)^2-l^2}}\right]. \tag{2-B.10}$$

When this expression is substituted into (2-B.5), the integration over ϕ' can be carried out explicitly, viz.,

$$\int_0^{2\pi} d\phi' J_0(\lambda\rho^*)=\int_0^{2\pi} d\phi' J_0\left(\lambda\sqrt{\rho^2+\rho'^2-2\rho\rho'\cos\phi'}\right)=2\pi J_0(\lambda\rho)J_0(\lambda\rho'). \tag{2-B.11}$$

As a consequence, we have

$$\Psi(\rho,z,t)=\frac{1}{2\pi}\int_0^{\infty}\rho' d\rho'\frac{1}{2\pi}\int_0^{\infty}\chi d\chi J_0(\chi\rho')\int_0^{\infty}\phi_{ap}(\chi,\omega)e^{i\omega t}d\omega\int_0^{\infty}\lambda d\lambda 2\pi J_0(\lambda\rho)J_0(\lambda\rho')$$
$$\times\left[i\sqrt{(\omega/c)^2-\chi^2}\,\frac{e^{-iz\sqrt{(\omega/c)^2-\lambda^2}}}{\sqrt{(\omega/c)^2-\lambda^2}}\right]. \tag{2-B.12}$$

We use next the orthogonality property

$$\frac{\delta(\chi-\lambda)}{\lambda}=\int_0^{\infty}\rho' d\rho' J_0(\chi\rho')J_0(\lambda\rho'). \tag{2-B.13}$$

Substituting (2-B.13) in (2-B.12) and integration over λ, we obtain

$$\Psi(r,z,t)=\frac{1}{2p}\int_0^{\infty}\int_0^{\infty} f_{ap}(c,w)c\,J_0(cr)e^{iwt}e^{-i\sqrt{(w/c)^2-c^2}z}dc\,dw, \tag{2-B.14}$$

which is the desired Weyl representation of the radiated field $(\omega/c>\chi)$ in the region $z>0$. Thus, the Rayleigh-Sommerfeld integral I representation given in (2-B.2) provides an exact solution to the 3-D scalar wave equation. As a consequence, it can be applied to the reconstruction of localized wave pulses at any distance z in front of the aperture. Its

equivalence to the positive frequency Weyl representation has been established only in the absence of acausal exciting field components at the source plane. In other words, the Rayleigh-Sommerfeld integral I representation incorporates acausal components, in contradistinction to Huygens' method. In the case of localized wave pulses, the acausal components can be minimized by tweaking the available free parameters.

Appendix 2-C

The Equivalence of the Rayleigh-Sommerfeld Integral II and Weyl Representations of the Solution to the 3-D Scalar Wave Equation

The Rayleigh-Sommerfeld integral II representation of the solution $\Psi(\mathbf{r},t)$ to the scalar wave equation [cf. Eq. (2-A.1)] inside a wavefront surface (zero field outside) is given as follows [153]:

$$\Psi(\mathbf{r},t)=\frac{1}{2\pi}\oint_S dS'\left\{-\frac{1}{R}\frac{\partial\Psi(\mathbf{r}',t')}{\partial n'}+\frac{1}{cR}\frac{\partial\Psi(\mathbf{r}',t')}{\partial t'}\frac{\partial}{\partial n'}(R)\right\}_{t'=t-R/c}. \tag{2-C.1}$$

Choosing S to be the aperture plane $z=0$ and assuming axisymmetry $\left[\Psi(\mathbf{r},t)=\Psi(\rho,z,t)\right]$, (2-C.1) specializes to

$$\Psi(\rho,z,t)=\frac{1}{2\pi}\int_0^{2\pi}d\phi'\int_0^{\infty}\rho' d\rho'\frac{1}{R}\left\{\frac{z}{cR}\frac{\partial\Psi(\rho',0,t')}{\partial t'}+\frac{z}{R^2}\Psi(\rho',0,t')\right\}_{t=t-R/c}, \tag{2-C.2}$$

where $R=\sqrt{\rho^2+\rho'^2-2\rho\rho'\cos\phi'+z^2}$. Our goal is to show that under certain conditions (2-C.2) is equivalent to the positive frequency Weyl representation [cf.(2-A.4)], viz.,

$$\Psi(\rho,z,t)=\frac{1}{2\pi}\int_0^{\infty}\int_0^{\infty}\phi(\chi,\omega)\chi J_0(\chi\rho)e^{i\omega t}e^{-i\sqrt{(\omega/c)^2-\chi^2}z}d\chi d\omega\,,\ z>0\,, \tag{2-C.3}$$

where $\phi_{ap}(\chi,\omega)$ denotes the spatio-temporal spectrum on the aperture plane $(z=0)$ $\phi_{ap}(\chi,\omega)\Leftrightarrow\Psi(\rho,0,t)$. We use, next, (2-C.3) in order to compute the value of the quantities $(\partial/\partial t')\Psi(\rho',0,t')$ and $\Psi(\rho',0,t')$ required in the Rayleigh-Sommerfeld integral II representation. Specifically, we obtain

$$\frac{\partial\left(\Psi\left(\rho',0,t'\right)\right)}{\partial t'}=\frac{1}{2\pi}\int_0^\infty d\omega\int_0^\infty i\omega\chi d\chi J_0\left(\chi\rho'\right)e^{i\omega t'}\phi_{ap}\left(\chi,\omega\right),\tag{2-C.4}$$

$$\Psi\left(\rho',0,t'\right)=\frac{1}{2\pi}\int_0^\infty d\omega\int_0^\infty d\chi\,\chi J_0\left(\chi\rho'\right)e^{i\omega t'}\phi_{ap}\left(\chi,\omega\right),\tag{2-C.5}$$

Inserting Eqs.(2-C.4) and (2-C.5) into (2-C.2), this leads to

$$\Psi\left(\rho,z,t\right)=\frac{1}{2\pi}\int_0^{2\pi}d\phi'\int_0^\infty\rho' d\rho'\Psi_1\left(\rho',z,t'\right),\tag{2-C.6}$$

where

$$\Psi_1\left(\rho',z,t'\right)=\frac{1}{2\pi}\int_0^\infty\chi d\chi J_0\left(\chi\rho'\right)\int_0^\infty\phi_{ap}\left(\chi,\omega\right)e^{i\omega t'}\frac{1}{R}\left[\frac{i\omega z}{cR}+\frac{z}{R^2}\right]_{t'=t-R/c}d\omega.\tag{2-C.7}$$

Next, we make use of the identity

$$\frac{\partial}{\partial z}\left[\frac{e^{-i\omega R/c}}{R}\right]=-\left[\frac{i\omega z}{cR^2}+\frac{z}{R^3}\right]e^{-i\omega R/c}.\tag{2-C.8}$$

As a consequence, Eq.(2-C.6) takes the form

$$\Psi\left(\rho,z,t\right)=\frac{-1}{(2\pi)^2}\int_0^{2\pi}d\phi'\int_0^\infty\rho' d\rho'\int_0^\infty\chi d\chi J_0\left(\chi\rho'\right)\int_0^\infty d\omega\phi_{ap}\left(\chi,\omega\right)e^{i\omega t}\frac{\partial}{\partial z}\left[\frac{e^{-i\omega R/c}}{R}\right].\tag{2-C.9}$$

Consider, next, the identity

$$\frac{e^{-i\omega R/c}}{R}=\int_0^\infty\lambda d\lambda J_0\left(\lambda\rho^*\right)I(\lambda,z),\tag{2-C.10}$$

where $\rho^*=\sqrt{\rho^2+\rho'^2-2\rho\rho'\cos\phi'}$ and $I(\lambda,z)$ is defined in (2-B.9). Proceeding as in Appendix 2-B, we obtain

$$\frac{\partial}{\partial z}\left[\frac{e^{-i\omega R/c}}{R}\right] = \int_0^\infty \lambda d\lambda J_0\left(\lambda\rho^*\right)\frac{\partial}{\partial z}\left[I(\lambda,z)\right]$$
$$= -\int_0^\infty \lambda d\lambda J_0\left(\lambda\rho^*\right)e^{-iz\sqrt{(\omega/c)^2-\lambda^2}} \tag{2-C.11}$$

for the region $z > 0$. Substituting (2-C.11) into (2-C.9), we have

$$\Psi(\rho,z,t) = \frac{1}{(2\pi)^2}\int_0^\infty \rho' d\rho' \int_0^\infty \chi d\chi J_0(\chi\rho') \int_0^{2\pi} d\phi' \int_0^\infty d\omega \phi_{ap}(\chi,\omega)e^{i\omega t}$$
$$\times \int_0^\infty \lambda d\lambda J_0\left(\lambda\rho^*\right)e^{-iz\sqrt{(\omega/c)^2-\lambda^2}}. \tag{2-C.12}$$

We carry out the integration over ϕ' using the formula in (2-B.11); as a result, we obtain

$$\Psi(\rho,z,t) = \frac{1}{(2\pi)^2}\int_0^\infty \rho' d\rho' \int_0^\infty \chi d\chi J_0(\chi\rho') \int_0^\infty d\omega \phi_{ap}(\chi,\omega)e^{i\omega t} \int_0^\infty \lambda d\lambda 2\pi J_0(\lambda\rho')$$
$$\times J_0(\lambda\rho)e^{-iz\sqrt{(\omega/c)^2-\lambda^2}}. \tag{2-C.13}$$

We use, next, the orthogonality property in (2-B.13) and integrate over λ. The final expression for $\Psi(\rho,z,t)$ is given as follows:

$$\Psi(\rho,z,t) = \frac{1}{2\pi}\int_0^\infty \int_0^\infty \phi_{ap}(\chi,\omega)\chi J_0(\chi\rho)e^{i\omega t}e^{-i\sqrt{(\omega/c)^2-\chi^2}z} d\chi d\omega. \tag{2-C.14}$$

This is the Weyl representation of the exact solution to the 3-D scalar wave equation. This proof shows that the Rayleigh-Sommerfeld integral II representation is equivalent to the Weyl representation only if the causal components of the exciting field are considered at the aperture plane. In general, the Rayleigh-Sommerfeld integral II representation incorporated acausal components. In the case of localized wave pulses, the latter can be minimized by tweaking the available free parameters.

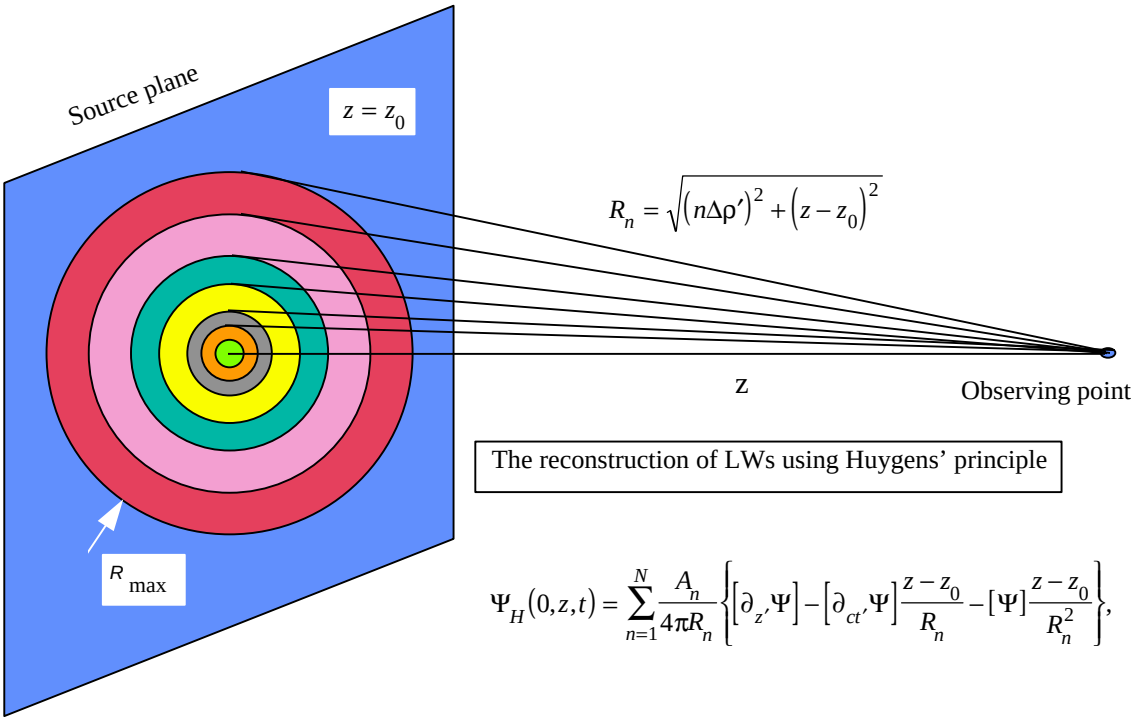

Figure 2.1: Geometrical configuration of the source plane and the discrete annular sections for launching a localized wavefield.

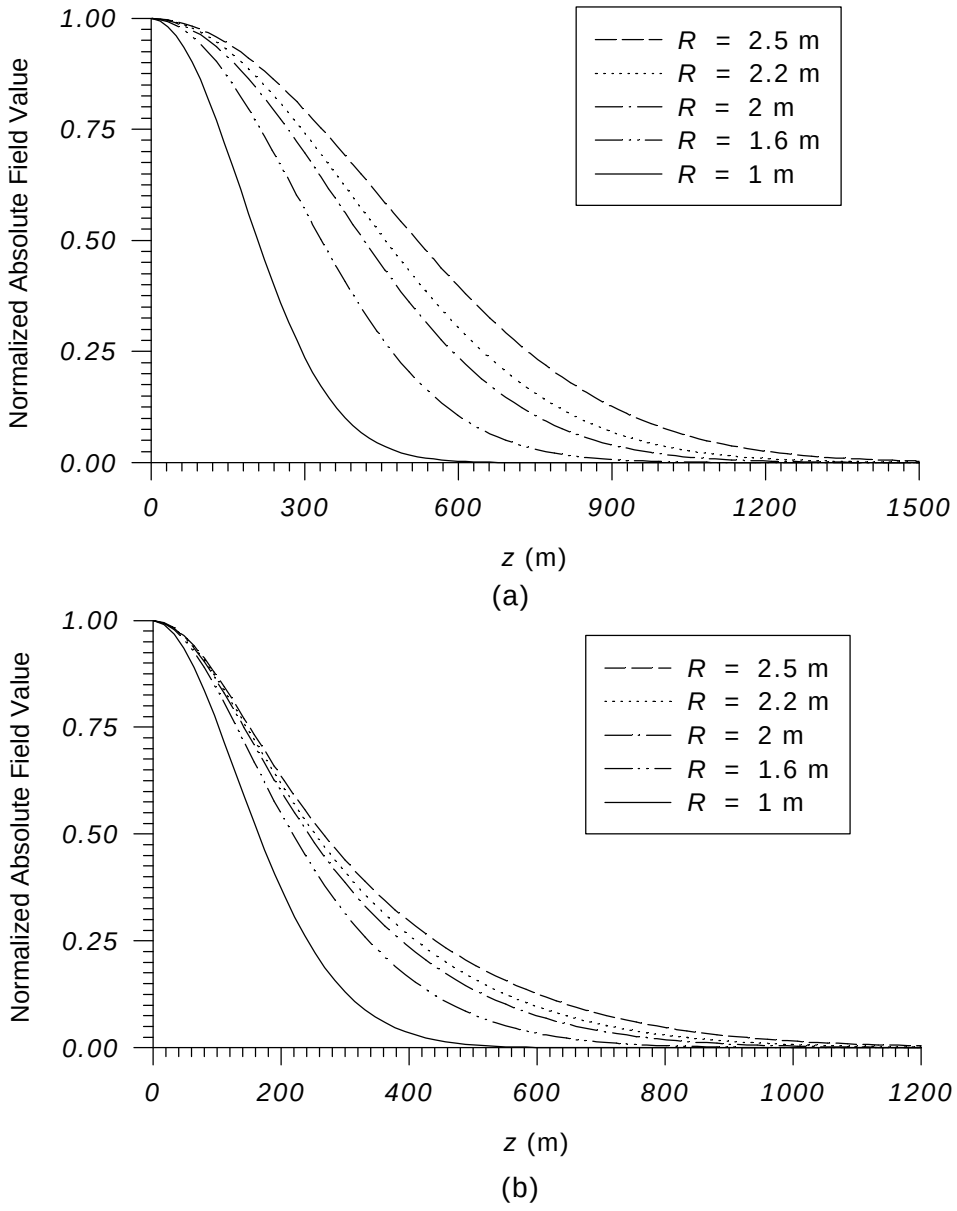

Figure 2.2: Decay of the centroid field value obtained by discrete arrays (a) FWM pulse; (b) MPS pulse.

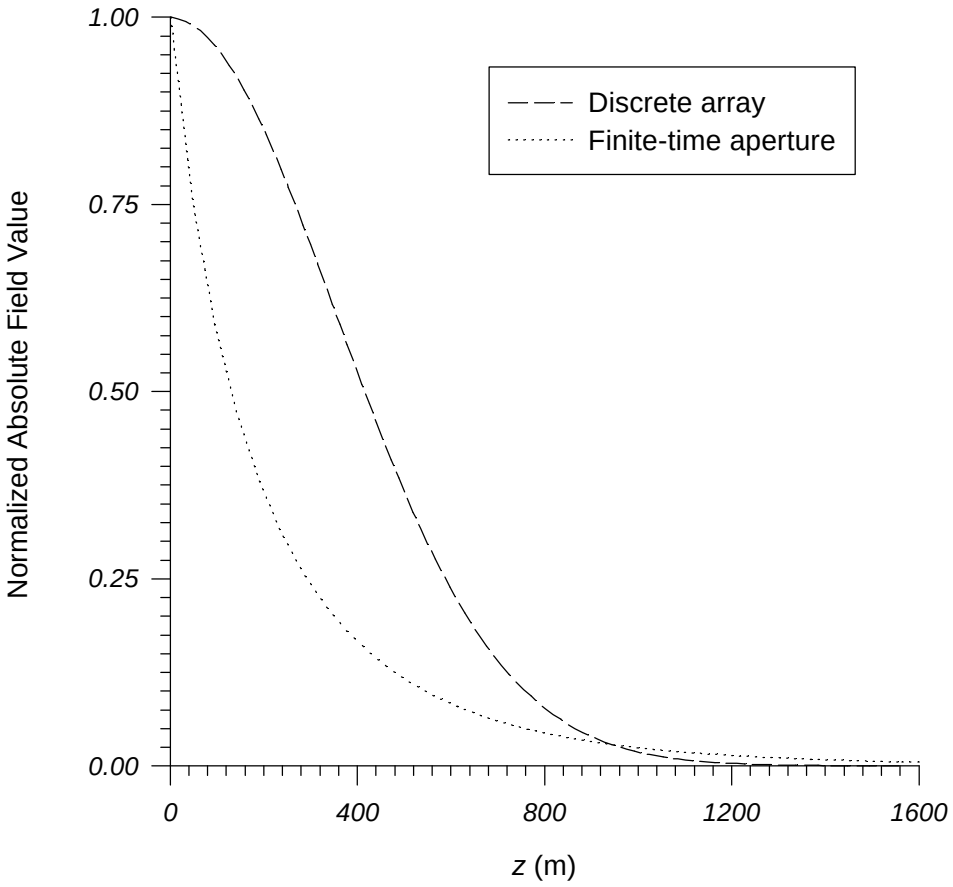

Figure 2.3: Decay of the centroid field value of a FWM in the case of discrete arrays using Huygens' principle and a TLFWM using the Weyl representation.

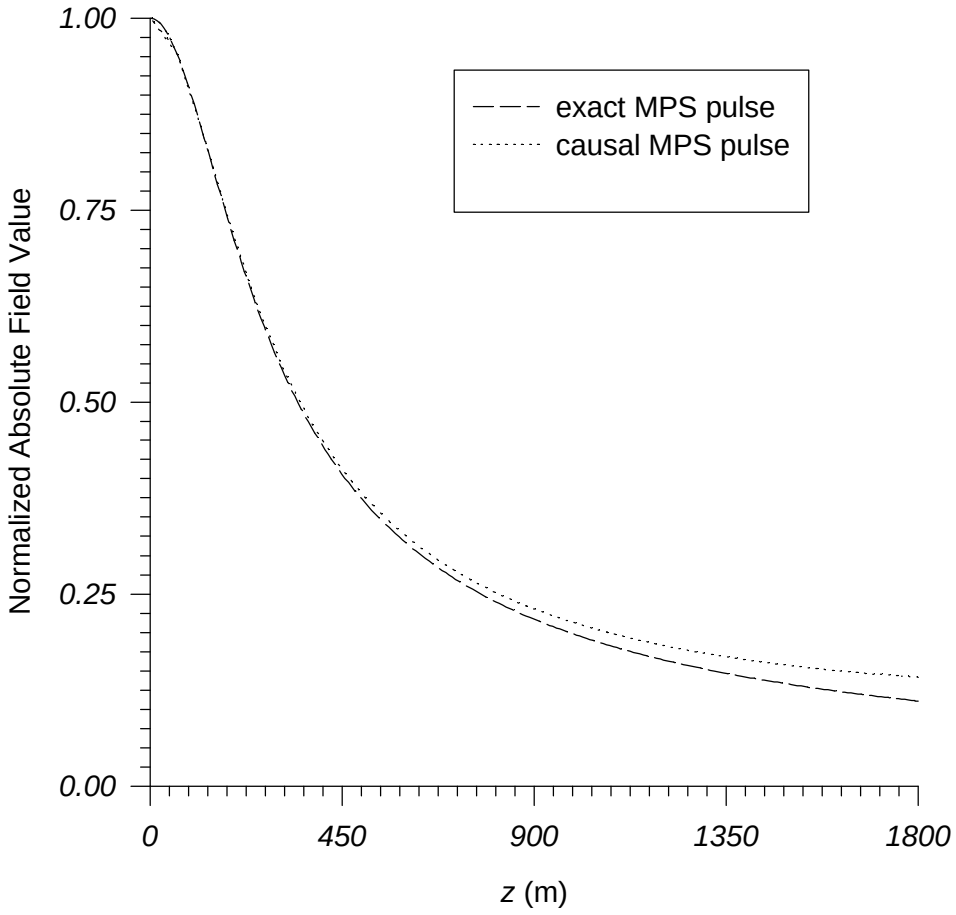

Figure 2.4: Comparison between the decay of the exact MPS and the causal one obtained from the Weyl representation.

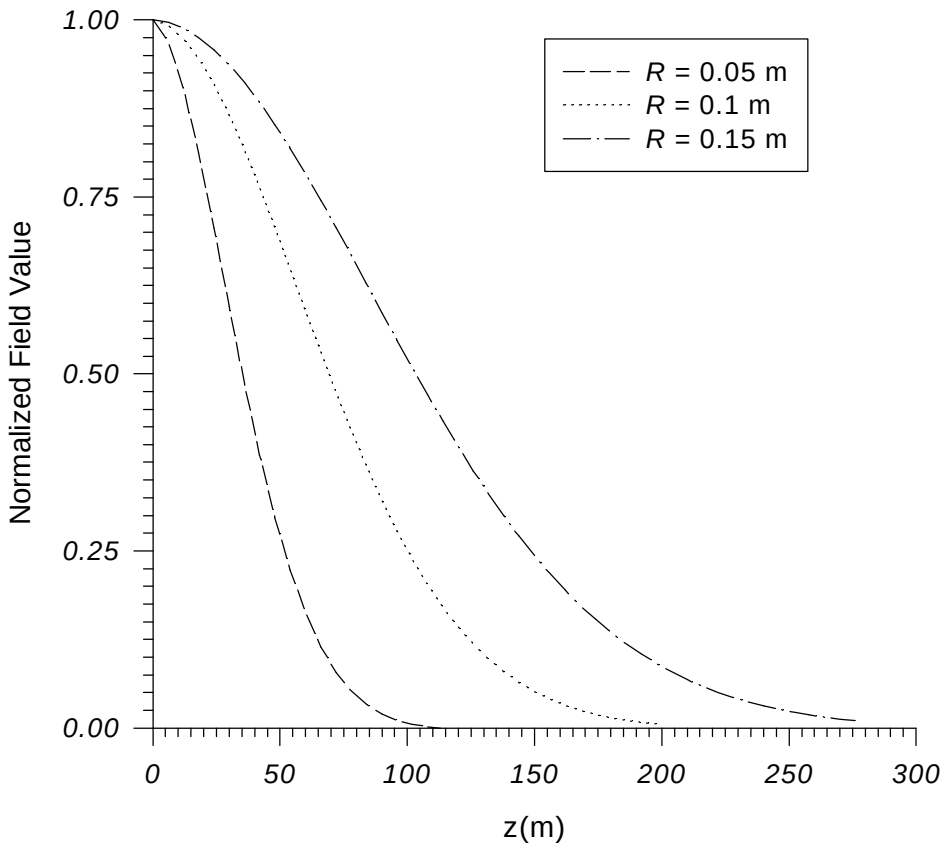

Figure 2.5: The decay of the centroid field value of a zeroth-order X wave for different radii.

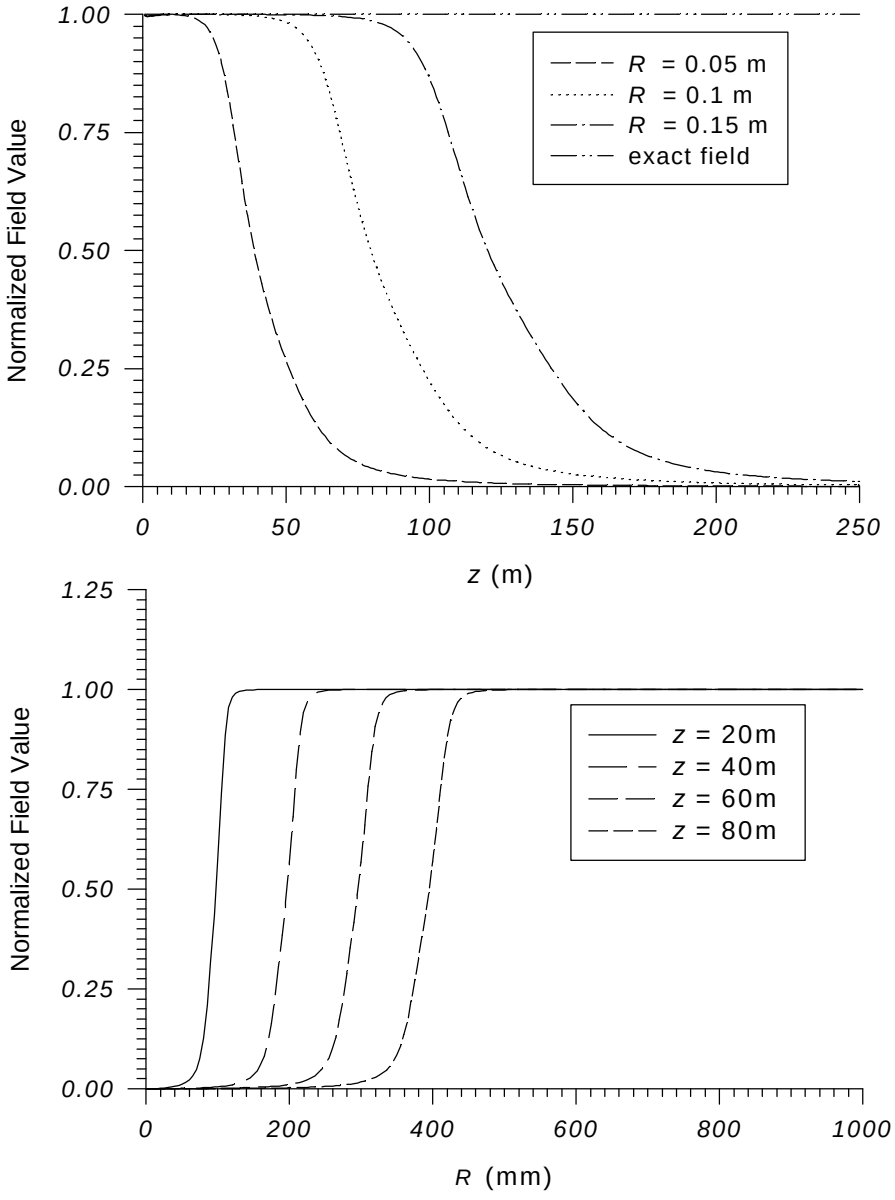

Figure 2.6: The variation of the normalized field value of a zeroth-order X wave with distance z in the upper graph and with the radius of the discrete arrays (R) in the lower one.

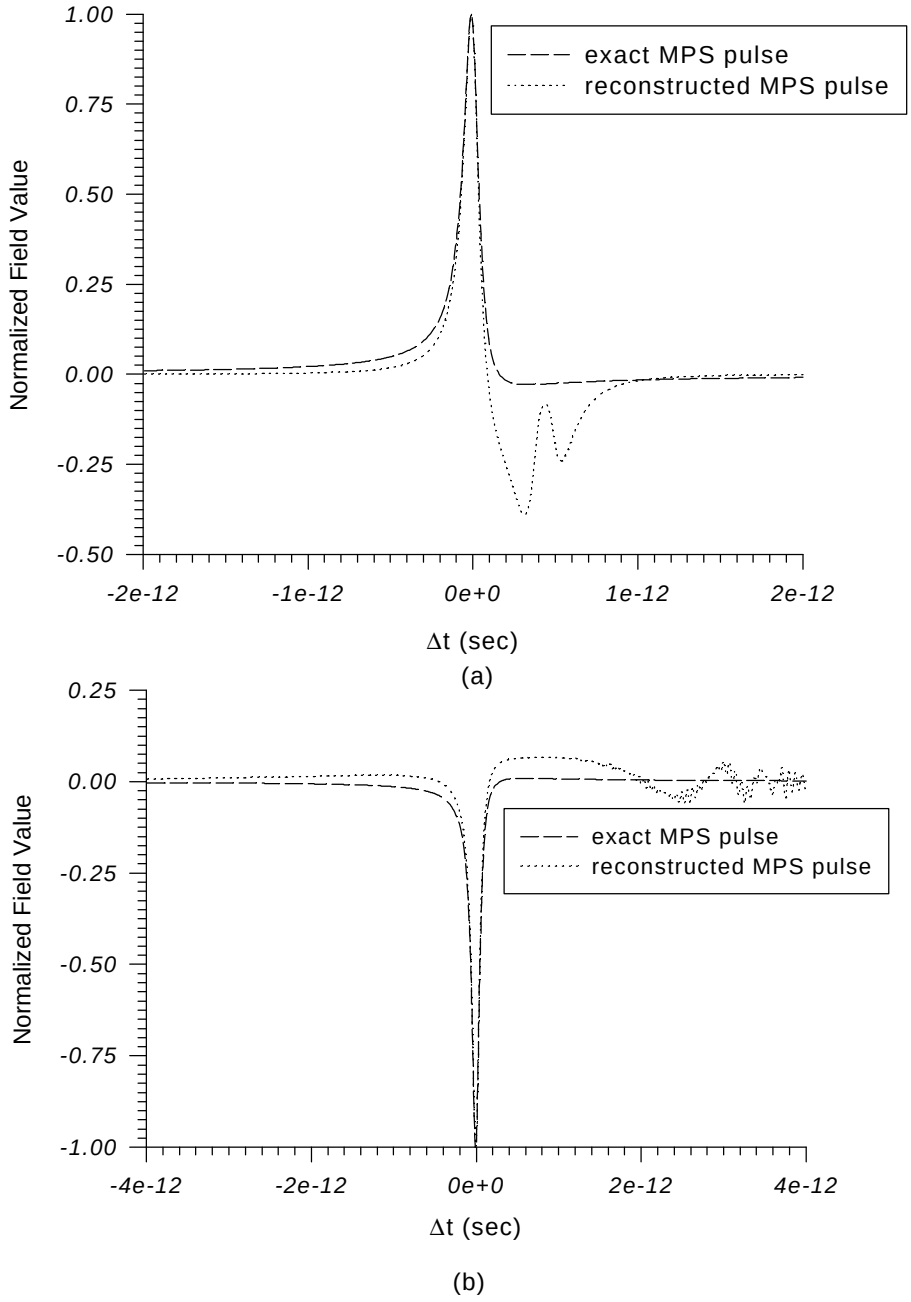

Figure 2.7: Comparison between the exact MPS pulse and one reconstructed using the Rayleigh-Sommerfeld integral I representation:
(a) $z = 1$ km; (b) $z = 10$ km

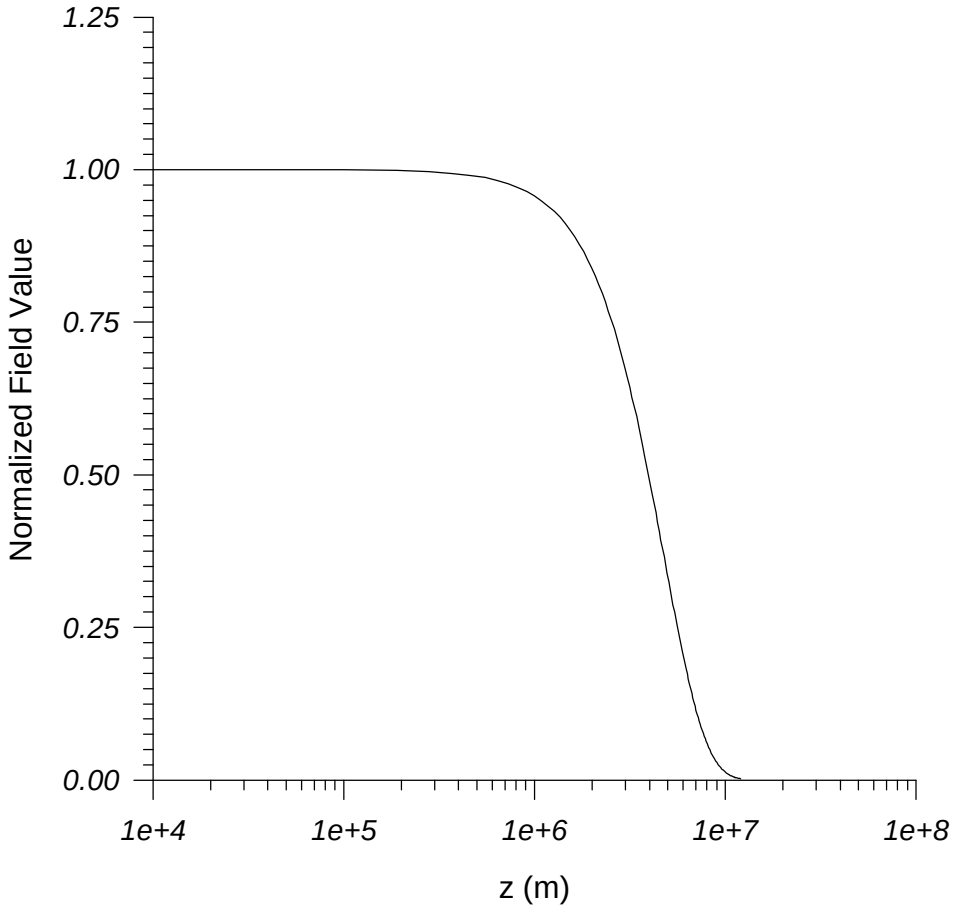

Figure 2.8: The decay of the centroid of the MPS pulse. The maximum radius of the source equals 5 m.

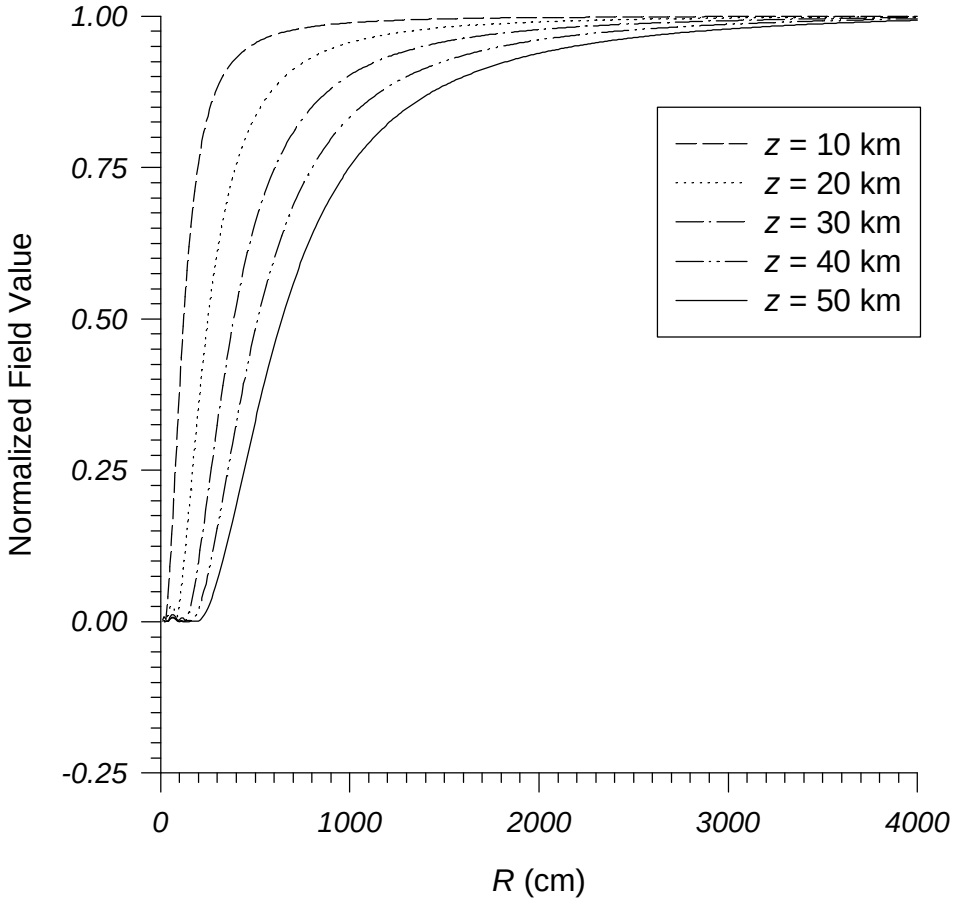

Figure 2.9: The dependence of the field amplitude for the MPS pulse on contributions from various radial elements.

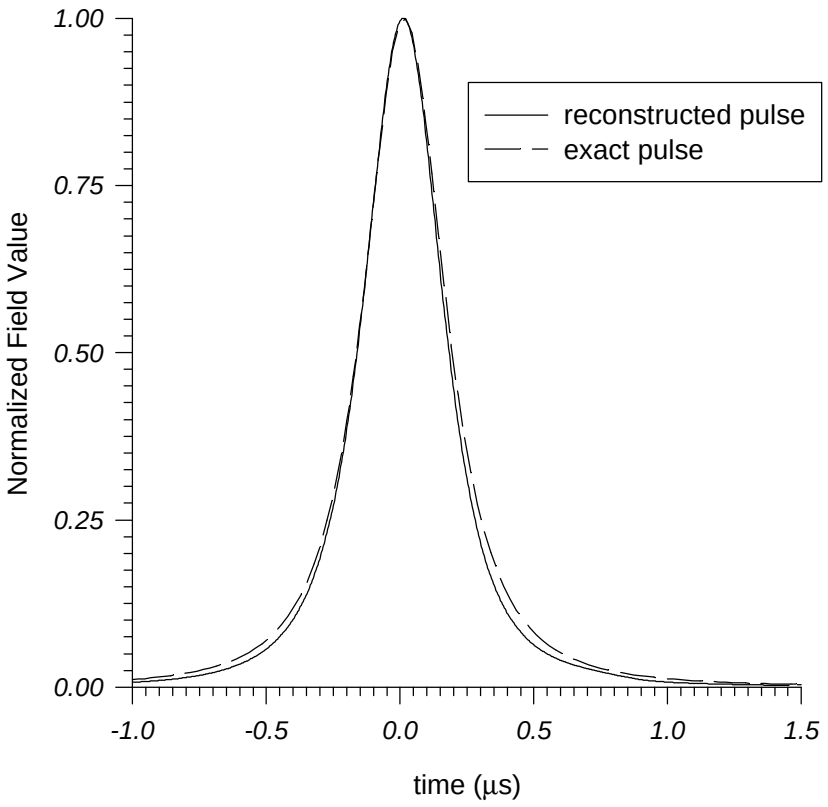

Figure 2.10: A comparison between the time history of the second derivative X wave pulse and the exact one.

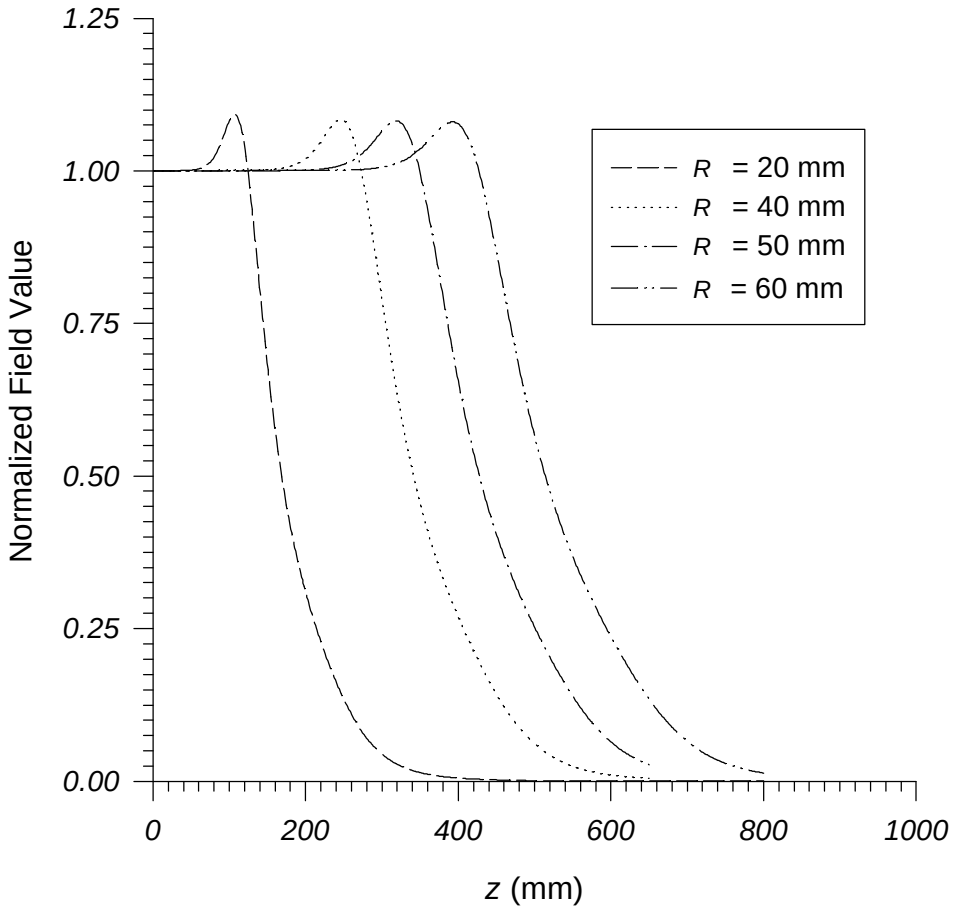

Figure 2.11: The decay of the absolute value of the centroid of the second derivative X wave derived for sources of different radii.

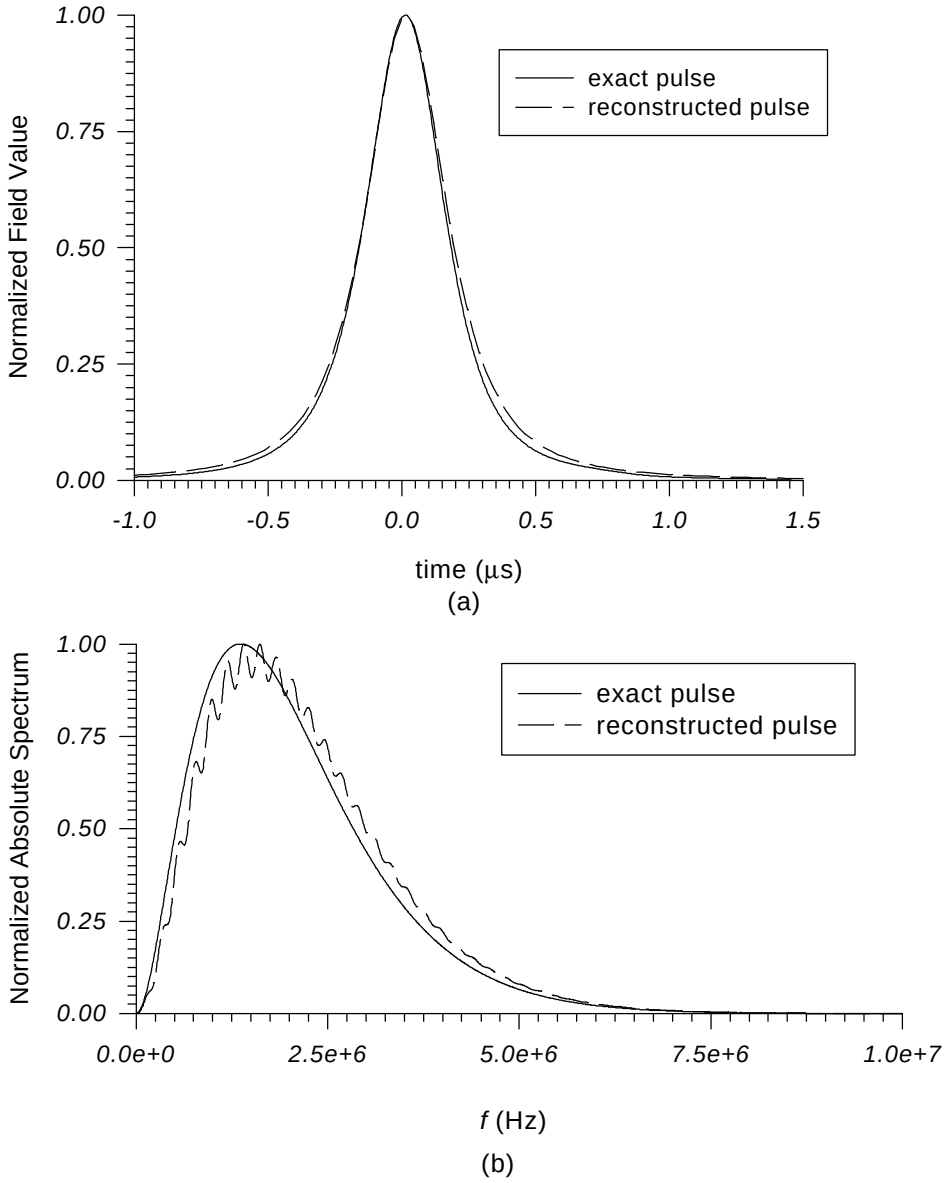

Figure 2.12: Comparison between the reconstructed second derivative X wave and the exact one at $z = 200$ mm and $\rho = 0$. The reconstruction has been carried out in the frequency domain using the Rayleigh-Sommerfeld integral II representation: (a) time domain; (b) frequency domain.